Planetary and Space Science 59 (2011) 456–467

Contents lists available at ScienceDirect

Planetary and Space Science

journal homepage: www.elsevier.com/locate/pss

Foreshock cavities and internal foreshock boundaries

Laurence Billingham [a,*,1], Steven J. Schwartz [a], Mark Wilber [b]

[a] Space and Atmospheric Physics, Blackett Laboratory, Imperial College London, London, UK
[b] Space Sciences Laboratory, University of California, Berkeley, USA

ARTICLE INFO

Article history:
Received 28 August 2009
Received in revised form
20 January 2010
Accepted 25 January 2010
Available online 2 February 2010

Keywords:
Foreshock
Upstream waves and particles
Ion kinetic effects
Bow shock
Planetary magnetosphere
Space plasma

ABSTRACT

We present two case studies of cluster encounters with foreshock cavities. For one event, we are able, for the first time, to accurately relate the observation of a foreshock cavity to the measured position of the bow shock. This allows us to compute the shock angle, a vital parameter in models of foreshock cavity formation, with greater confidence than any previous study. This cavity appears to be elongated along the magnetic field and we use the multispacecraft nature of the Cluster mission to constrain its field-parallel and -perpendicular extent. We show that this event is embedded within a region of field-aligned ion beams. This is the first time a foreshock cavity has been shown to be surrounded by foreshock ion beams. A second foreshock cavity is associated with a small rotation in the interplanetary magnetic field (IMF). We show that this event appears on the boundary between an interval when the spacecraft were inside the ion foreshock, and an excursion upstream. This is the first report of a foreshock cavity observed during the traversal of the global foreshock. This second event has some features expected from the new Sibeck et al. (2008) model of cavities as brief encounters with a spatial boundary in the global foreshock.

1. Introduction

The foreshock region upstream of and magnetically connected to the bow shock is permeated by particles streaming from the shock against the flow of the solar wind (see Eastwood et al., 2005, for a recent review). Many foreshock phenomena can be organised by θ_{Bn}, the angle between the upstream magnetic field and the normal to the shock surface at their point of intersection.

The field aligned beam (FAB) region ($70^\circ \gtrsim \theta_{Bn} \gtrsim 40^\circ$) forms a narrow layer characterised by beams of backstreaming ions with energies of a few to 15 keV that lacks significant wave activity (Meziane et al., 2005a; Bonifazi and Moreno, 1981b, 1981a; Paschmann et al., 1981). These ions are thought to escape from the part of the reflected ring distribution immediately in front of the shock (Möbius et al., 2001).

A short distance downstream, populations of gyrating (finite pitch angle) ions are found with energies < 40 keV (Meziane et al., 2001; Fuselier et al., 1986). The region dominated by these ions is know as the intermediate ion foreshock. The quasi-monochromatic Ultra Low Frequency (ULF) waves found in this region are thought to form due to instabilities caused by FABs streaming against the solar wind. Wave particle interactions scatter the FABs, forming the distributions of gyrating ions (Mazelle et al., 2005, 2003; Meziane et al., 2001).

Further downstream ($\theta_{Bn} \lesssim 40^\circ$) lies a region of isotropic ions whose energy spectrum extends to ≥ 100 keV. These diffuse ions are observed accompanied by steepened, turbulent ULF waves (Paschmann et al., 1981; Scholer, 1995; Trattner et al., 1994; Gosling et al., 1989).

For quasi-steady upstream conditions, the large-scale structure the foreshock is as outlined above. However, changes in the Interplanetary Magnetic Field (IMF) direction will cause the whole foreshock to move as θ_{Bn} changes. A variety of smaller, transient, phenomena can also be found in the upstream region (see Wilber et al., 2008, for an overview).

Hot Flow Anomalies (HFAs) form when a subset of solar wind discontinuities interact with the bow shock (Schwartz et al., 2000). Ions that have been reflected at the shock are channelled onto the discontinuity. HFAs are characterised by large changes in the plasma bulk flow, strong heating and perturbations in magnetic field and particle density (Lucek et al., 2004).

Density holes (Parks et al., 2006; Wilber et al., 2008) are sub-minute duration events that share some features with HFAs. The solar wind beam within density holes and early stage HFAs is disrupted and partially replaced by isotropic suprathermal ions, well-developed HFAs are marked by a single isotropic ion distribution. HFAs and density holes are associated with enhancements in wave activity (Tjulin et al., 2008; Lin et al., 2008) and

* Corresponding author. Tel.: +44 20 7594 1354.
E-mail address: laurence.billingham01@imperial.ac.uk (L. Billingham).
[1] Current address: Impacts and Astromaterials Research Centre, Department of Earth Science and Engineering, Imperial College London, London, UK.

0032-0633/$ - see front matter © 2010 Elsevier Ltd. All rights reserved.
doi:10.1016/j.pss.2010.01.012

often appear as cavities of depleted magnetic field magnitude and thermal particle density. Like HFAs, density holes are associated with changes in the large scale IMF, however, the magnetic shears across density holes are usually smaller than those (typically $\sim 60^{\circ}$) associated with HFAs and the magnitude of the magnetic shear is not well correlated with density hole depth. Wilber et al. (2008), in a survey of 37 density holes, found that the bulk flow deviations within density holes tend to be smaller than those in HFAs. Typically, the normal components of the motional electric field at the current sheets which bound density holes tend to point outward; whereas most HFAs have an inward pointing electric field on at least one side (Schwartz et al., 2000).

Foreshock cavities, like density holes and some HFAs, are marked by central decreases in magnetic field magnitude and thermal ion density, often bounded by enhancements at the cavity edges (Billingham et al., 2008). They do not, however, exhibit strong flow deflections or heating of the bulk ion population. However, they are associated with a second, suprathermal, ion population (Wibberenz et al., 1985; Sibeck et al., 2001; Schwartz et al., 2006; Billingham et al., 2008).

Most studies of foreshock cavities have assumed them to be generated on field lines that are well connected to the bow shock but embedded within a region of disconnected plasma (see e.g. Sibeck et al., 2002; Schwartz et al., 2006). The local hybrid simulation of Thomas and Brecht (1988) reproduced the features characteristic of foreshock cavities: crater-like depressions, observed in magnetic field magnitude and thermal particle density, filled with energetic ions.

The magnetic field and density profiles found by Skadron et al. (1986) for the traversal of a model foreshock resemble those observed for foreshock cavities. It has been suggested, by Sibeck et al. (2008) on the basis of a global hybrid simulation, that foreshock cavities might be transient encounters with the moving ion foreshock sweeping back and forth over a spacecraft.

Blanco-Cano et al. (2009), using similar global hybrid simulations, identify foreshock cavity-like events embedded within the ULF foreshock. These foreshock cavitons have been seen to occur in the Cluster dataset. The example shown by Blanco-Cano et al. (2009) appears to be considerably smaller, in solar wind convected width, than typical isolated foreshock cavities (e.g. Billingham et al., 2008). It is suggested that, in the 2D simulation, foreshock cavitons may form from the interaction between two different types of waves in the ULF wave-field. Based on this suggestion Blanco-Cano et al. (2009) regard cavitons as a distinct class of events rather than simply foreshock cavities embedded within the ULF region.

The survey of Billingham et al. (2008) showed that foreshock cavities are not co-located with the nominal upstream edge of the intermediate ion foreshock. However, they were not able to definitively discriminate between the edge encounter and locally anomalous connection models of foreshock cavity formation. Billingham et al. (2008) state that future work should focus on locating foreshock cavities with respect to the bow shock and relevant upstream particle boundaries.

On 4 February 2006 the Cluster spacecraft observed two foreshock cavities. For the first event, encountered at 05:37 (UT), we are able to exploit the multi-spacecraft nature of the Cluster mission. One of the quartet crosses the bow shock as others observe the cavity. This simultaneous shock encounter is the first that has been reported and is unique in the Billingham et al. (2008) set of Cluster foreshock cavities. For the first time, we are able to definitively locate a foreshock cavity with respect to measured shock position. This enables us to calculate the shock geometry (a vital parameter in cavity formation models) with more certainty than in previous studies which have inferred the location of the bow shock. The locations of cavity-observing spacecraft relative to those that miss the event allow us to constrain the cavity's size perpendicular to the magnetic field. The 05:37 foreshock cavity appears to be an isolated event. Solar wind conditions before and after the event are very similar and it appears that this event is consistent with the locally anomalous connection model. A second foreshock cavity occurred some four hours later at 09:33. It is substantially different in character from the first event, occurring on an obvious boundary between two differing plasma regimes. A small magnetic rotation changes the global shock connection of the field-line threading the spacecraft.

In this paper, we explore the contrasting signatures of these two events and compare them to expectations based on different models of foreshock cavity formation.

We use data from the Cluster mission taken during the morning of the 4th of February 2006 when the Cluster spacecraft were somewhat duskward of the subsolar bow shock and near the ecliptic plane. We take magnetic field data at spin and 5 Hz resolution from FGM (Balogh et al., 2001), 3D ion distributions and their moments from CIS(HIA) (Rème et al., 2001), spin resolution probe potential from EFW (Gustafsson et al., 1997) (this can be used as a proxy for plasma density e.g. Pedersen et al., 2001, 2008; Kellogg and Horbury, 2005) and high energy ion flux from RAPID (Wilken et al., 2001).

2. Isolated foreshock cavity 05:37

2.1. Overview

Fig. 1 gives an overview of the observations for the foreshock cavity centred at 05:37. When it observed the event Cluster 1 (C1) was located at (12.5, 10.3, 1.1) R_E GSE, close to the position of the bow shock; inter-spacecraft separations were $\leq 1.8R_E$. C1 observes a foreshock cavity characterised by a dropout in magnetic field magnitude and EFW probe potential (and hence plasma density) with a partial recovery in the interior. The edges of the event have magnetic field strengths and densities elevated over the background level. Associated with the magnetic dropout, C1 observes enhanced fluxes of energetic ($E \gtrsim 10$ keV) ions. The onset of the observation of these ions coincides with the first magnetic edge enhancement. The ions persist for several minutes after the passage of the magnetically depleted region, in accordance with previous foreshock cavity observations. Sibeck et al. (2001) noted that enhanced fluxes of high energy ions often last longer than magnetic cavity signatures and enhanced suprathermal fluxes are observed outside the magnetic cavity of the event presented by Schwartz et al. (2006). These authors show that, outside of the central magnetically depleted region, the pressure of the suprathermal population is not high enough to excavate a cavity.

C2 also encounters the event; the first magnetic edge enhancement occurs ~ 2 s earlier at C2 than C1. The partial internal recovery is observed ~ 1.5 s later at C2 and it encounters the second edge enhancement ~ 25 s later than C1. Overall, the cavity interior at C2 lasts longer and is more highly structured than at C1.

C3 measures some field disturbance contemporary with the passage of foreshock cavity at the other spacecraft, but there is no significant coherent dropout in magnetic field magnitude or thermal ion density.

C4 encounters the bow shock multiple times during the interval of Fig. 1; a pair of shock crossings occur whilst C1 and C2 observe the foreshock cavity magnetic depletion. The (05:36:22) shock crossing a minute before the foreshock cavity is preceded by a distinct magnetic field signature. The field strength measured by C4 drops by a factor of ~ 3 and the field

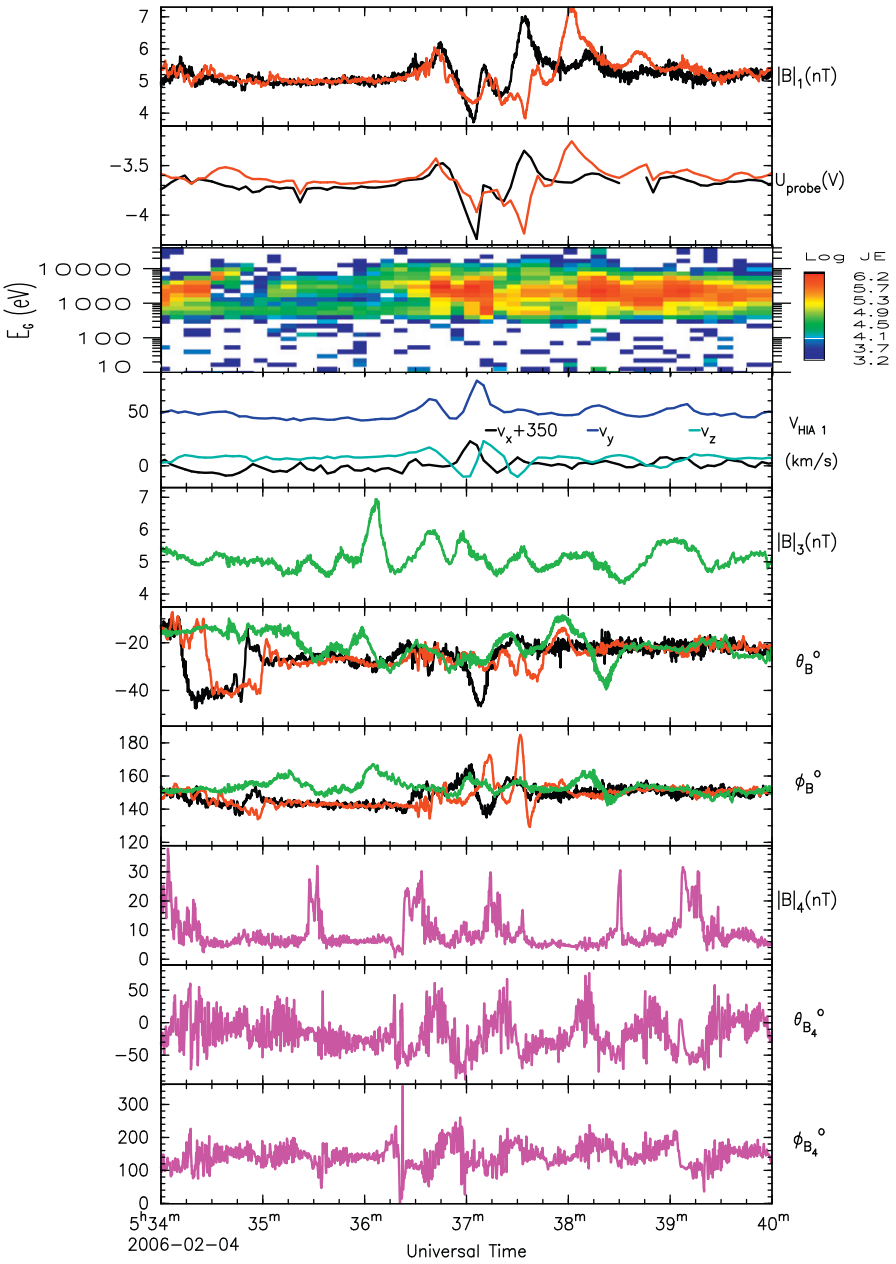

Fig. 1. Overview of the 2006-02-04 05:37 foreshock cavity. The panels show (from top down): magnetic field magnitude from Cluster 1 (C1) and Cluster 2, EFW probe potential from C1 and C2, an ion omni-directional time energy spectrogram from the high-G part of CIS(HIA) on C1, GSE components of the ion bulk flow from C1, field magnitude from C3, magnetic field latitudinal angle from C1 C2 and C3, C1 C2 C3 field azimuthal angle, field magnitude and angles from C4. Note that the vertical (nT) scale for C4 |**B**| (fourth panel from top) is ~10 times larger than that on the other |**B**| panels.

direction changes through an angle of ~150°; easily seen at 05:36:22 in the bottom (ϕ) panel of Fig. 1. Immediately afterwards, the bow shock advances over C4, possibly as a result of this change in the magnetic field. It is clear that the plasma environment upstream of the bow shock is highly structured on the scale (~10,000 km) of the Cluster inter-spacecraft separation. The bow shock crossing at C4 during the passage of the foreshock cavity at C1 and C2 is unique in the literature and in the set of cavities in the Billingham et al. (2008) study.

Fig. 2 shows the configuration of the four Cluster spacecraft, in boundary normal coordinates, during the foreshock cavity encounter (05:37:08). The $\hat{n}$ direction is calculated by scaling the bow shock model of Slavin and Holzer (1981) to the position of C4. The $\hat{l}$ vector lies parallel to the shock surface such that the ln plane contains the magnetic field vector measured by C1 contemporary with the minimal field magnitude.

The separation between C1 and C4, and hence the bow shock, is ~$0.4R_E$ along the shock normal direction; the corresponding

distance $(C2-C4)\cdot\hat{n}$ is $\sim 1R_E$. C1–C2 are separated by a total of $1.76R_E$. The angle separating the magnetic field and the line joining C1 to C2 is only $\sim 20^\circ$. Thus, these spacecraft lie approximately along the interior field direction. In contrast, the interior field and the line joining C1–C3 are separated by more than 70°. The perpendicular distance between C3 and the line joining C1 to C2 is $1.15R_E$ (this corresponds to one gyroradius for a ~ 40 keV proton in the cavity interior field or the gyroradius of a ~ 70 keV proton gyrating in the field measured at C3). The foreshock cavity scale inferred from the C1 and C2 observations is comparable to the solar wind convected width of this foreshock cavity ($2.7R_E$ at C1 and $4.3R_E$ at C2); but it is significantly less than the $\sim 8R_E$ average cavity convected width reported by Billingham et al. (2008).

Noting that C3 does not observe the foreshock cavity, we suggest that the event is elongated along the field direction, having a parallel/perpendicular aspect ratio of $\gtrsim 1.5$. However, note that the location of the opposite edge of the cavity cannot be constrained.

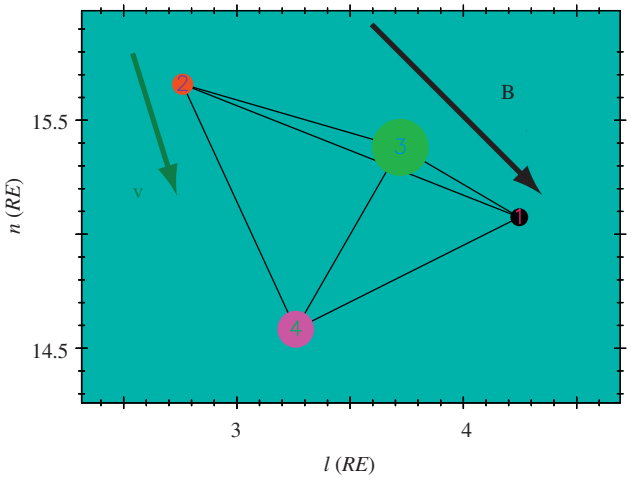

Fig. 2. Cluster spacecraft positions in boundary normal coordinates. The central minimum magnetic field measured by C1 $\mathbf{B}=(-3.6,2.5-1.3)\,nT_{GSE}$ is shown by the black arrow under the mapping $4\,nT\rightarrow 1R_E$. The projection of the solar wind flow measured by C3 onto the ln plane is shown by the green arrow under the mapping $0.1R_E\,s^{-1}\rightarrow 1R_E$. The relative sizes of the coloured circles represent spacecraft displacement perpendicular to the plane. (For interpretation of the references to colour in this figure legend, the reader is referred to the web version of this article.)

2.2. Shock geometry and ion signatures

Fig. 3 combines ion time-energy spectrograms, magnetic field data and shock geometry computed by tracing along the field to a model shock. According to the anomalous connection model of foreshock cavity formation (e.g. Schwartz et al., 2006), the energetic particles inside foreshock cavities are present because the field lines threading the centre of the event (and the observing spacecraft) connect to the quasi-parallel bow shock. In this section we take advantage of the position of C4 at the bow shock to find how the magnetic fields associated with the 05:37 event connect to the shock.

We have used the model of Slavin and Holzer (1981), scaled to the position of C4 at the shock, to examine the magnetic connection to the bow shock at various times during the foreshock cavity encounter.

Given the proximity of all spacecraft to the shock and the large radius of curvature of all shock models, the use of different

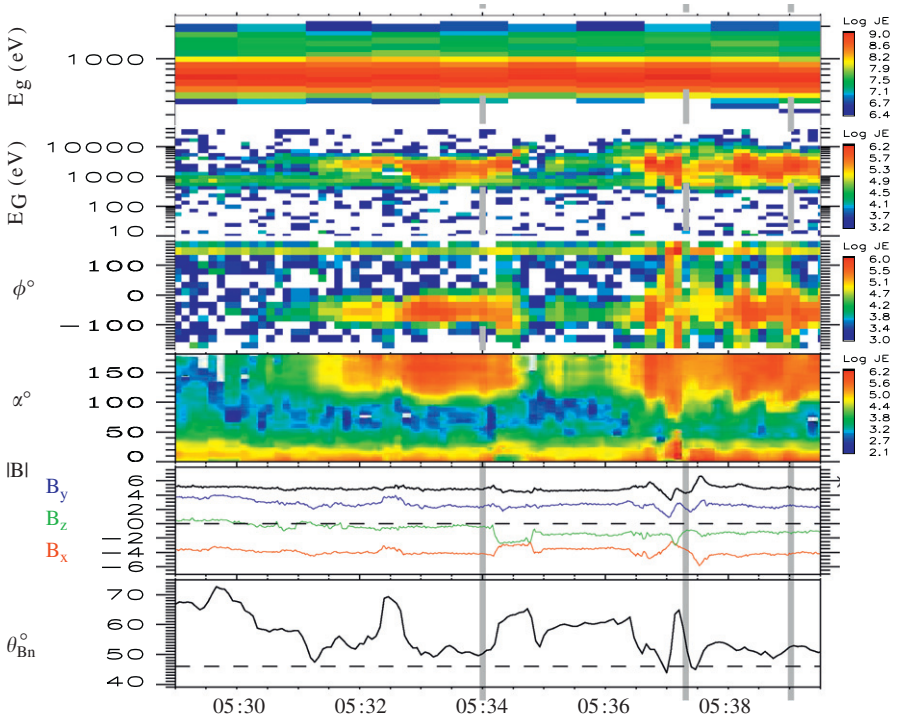

Fig. 3. Data taken by the CIS(HIA) instrument on C1 between 2006-02-04 05:29:00 and 05:39:30. Colour scales indicate the differential energy flux of ions. The first panel shows the solar wind beam measured by the low geometric factor sensor. Other spectra were taken from the high geometric factor sensor. The second panel shows an omnidirectional spectrum. The third panel is a latitudinal flow angle spectrogram. The fourth panel show azimuthal flow angle. The fifth and final spectral panel shows the pitch angle between an ion's velocity and the magnetic field, computed in the spacecraft frame of reference. The sixth panel shows FGM magnetic field magnitude GSE and components. The final panel shows the angle between the traced magnetic field and the model shock normal at the intersection of the model surface and the field. The three vertical grey lines show the locations of the three sets of ion distributions sketched in Fig. 4. These correspond to the times (and approximate durations) of the distribution cuts presented in Fig. 5. (For interpretation of the references to colour in this figure legend, the reader is referred to the web version of this article.)

models does not significantly change the computed shock angles. In the 5 min around the foreshock cavity the difference in the shock angles calculated from the models of Slavin and Holzer (1981), Peredo et al. (1995), Farris et al. (1991), and Formisano (1979) (see Schwartz, 1998; Merka et al., 2005, for discussions of different models and their accuracies) is $<1^{\circ}$.

The immediate pre- (05:35:50) and post-cavity (05:39:45) field directions lie within 7° of one another. Tracing to the shock along the field lines threading C1 and C2 shows that their connection points are less than $0.2R_E$ apart. The field at C3 intersects the shock within $0.5R_E$ of the C1 field shock-intersection point.

Seven minutes before the foreshock cavity, the magnetic field turns to point slightly southwards. The shock angle falls from $\sim 70^{\circ}$ (05:29:40) to $\sim 55^{\circ}$ (05:31:45) allowing ions from the bow shock to reach the spacecraft. This new ion population can be seen flowing dawnward and anti-parallel to the magnetic field, away from the bow shock, in the third and fourth panels of Fig. 3. Dawnward ion flux persists throughout the interval. A field rotation at 05:34 changes the shock geometry to $\gtrsim 60^{\circ}$. In response, the ion flux from the shock is reduced and the peak flux moves to higher energies.

As can be seen from Fig. 3, the parts of the cavity interior near to the magnetic minimum (at 05:37:12) contain the highest energy ion fluxes and are connected to the bow shock with $\theta_{Bn} \sim 45^{\circ}$. C1 is $\sim 1.0R_E$ up-field from the shock-intersection point of the interior field, compared to the $\sim 0.7R_E$ typical for the interval 05:33 to 05:39. The interior field intersects the shock $<1R_E$ from the shock-intersection point of the pre-event field and only $\sim 2.5R_E$ from the location of C4 at the shock surface.

The flux of suprathermal ions is most intense inside the foreshock cavity, but weaker fluxes of energetic ions are observed nearby outside. Energetic ions outside the magnetic depletion region have been reported by Schwartz et al. (2006) and Sibeck et al. (2001). It is thought that either the pressure of the exterior ions is not great enough to excavate the cavity further or that the instability (Gary, 1991) causing the cavity has not yet grown outside of the central depletion.

2.3. Kinetic signatures

Fig. 4 sketches the ion populations observed before, during and after the foreshock cavity. Each set of lines corresponds to a row of Fig. 5 which shows two spin snapshots of the ions measured by CIS(HIA) at the times indicated by the vertical lines in Fig. 3. Within each row of Fig. 5 the left-hand panel shows a velocity-space cut in the $\vec{v}_{\perp}$ frame. This frame is constructed such that the magnetic field direction points rightwards and the direction of the perpendicular component of the bulk flow (which is afterwards subtracted) points upwards. Fig. 5's other three columns correspond to cuts in two field-perpendicular planes taken at the three different field aligned speeds marked by coloured lines in the left column.

In Fig. 5, the solar wind beam appears as a narrow red spot (labelled SW in the top left panel) just right of centre in all the $\mathbf{v}_{\parallel} \times \mathbf{v}_{\perp}$ panels (left column). Likewise, each of these panels show Field Aligned Beams (labelled FAB in the top left panel). These are found in the anti-field aligned direction with speeds comparable to the solar wind speed. Their distribution is a few times broader, in the $\mathbf{v}_{\perp}$ direction, than that of the solar wind beam. The FABs also dominate the $\mathbf{v}_{SW}-800$ cuts in the third column, appearing as broad, centred, spots whose orange/red colours indicate high fluxes.

Before the foreshock cavity (top row of Fig. 5, red lines in Fig. 4) the only ions present belong either to the solar wind or to the FAB populations.

Inside the foreshock cavity (middle row of Fig. 5, purple lines in Fig. 4) another component is present; it can be seen in the $\mathbf{v}_{\parallel} \times \mathbf{v}_{\perp}$ panel as an arc extending from the region of the FABs towards higher field anti-parallel and perpendicular velocities. These same ions are clearly visible in the $\mathbf{v}_{\perp}(\mathbf{v}_{\parallel} = \mathbf{v}_{SW}-400)$ panel,

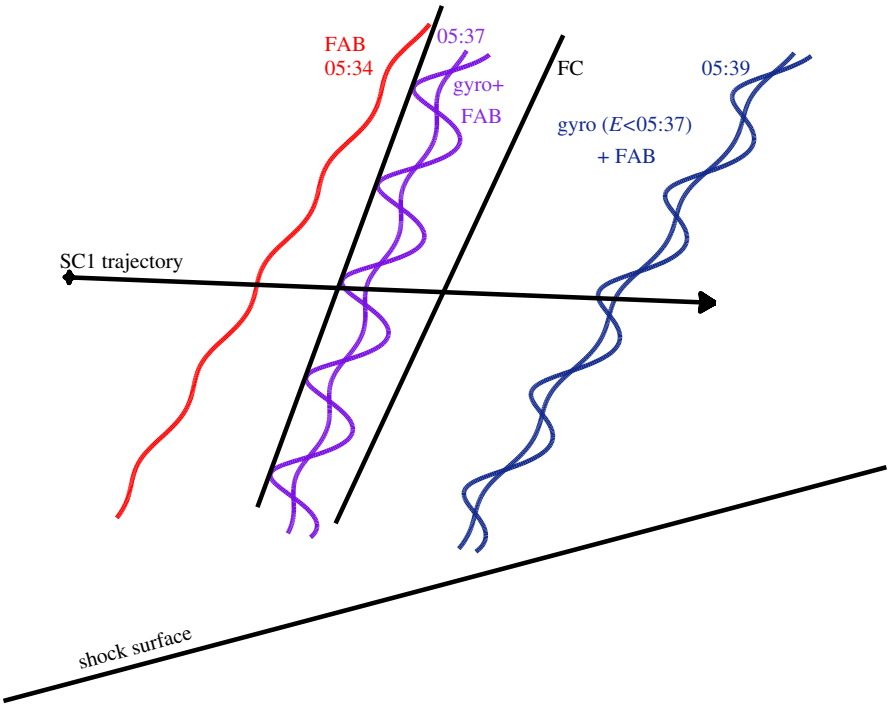

Fig. 4. A sketch of the different ion populations encountered by C1 between 05:34 and 05:39. The three populations correspond to the three cuts in Fig. 5. Note the change in the angle between the magnetic field and the shock surface from the inside to the outside of the cavity.

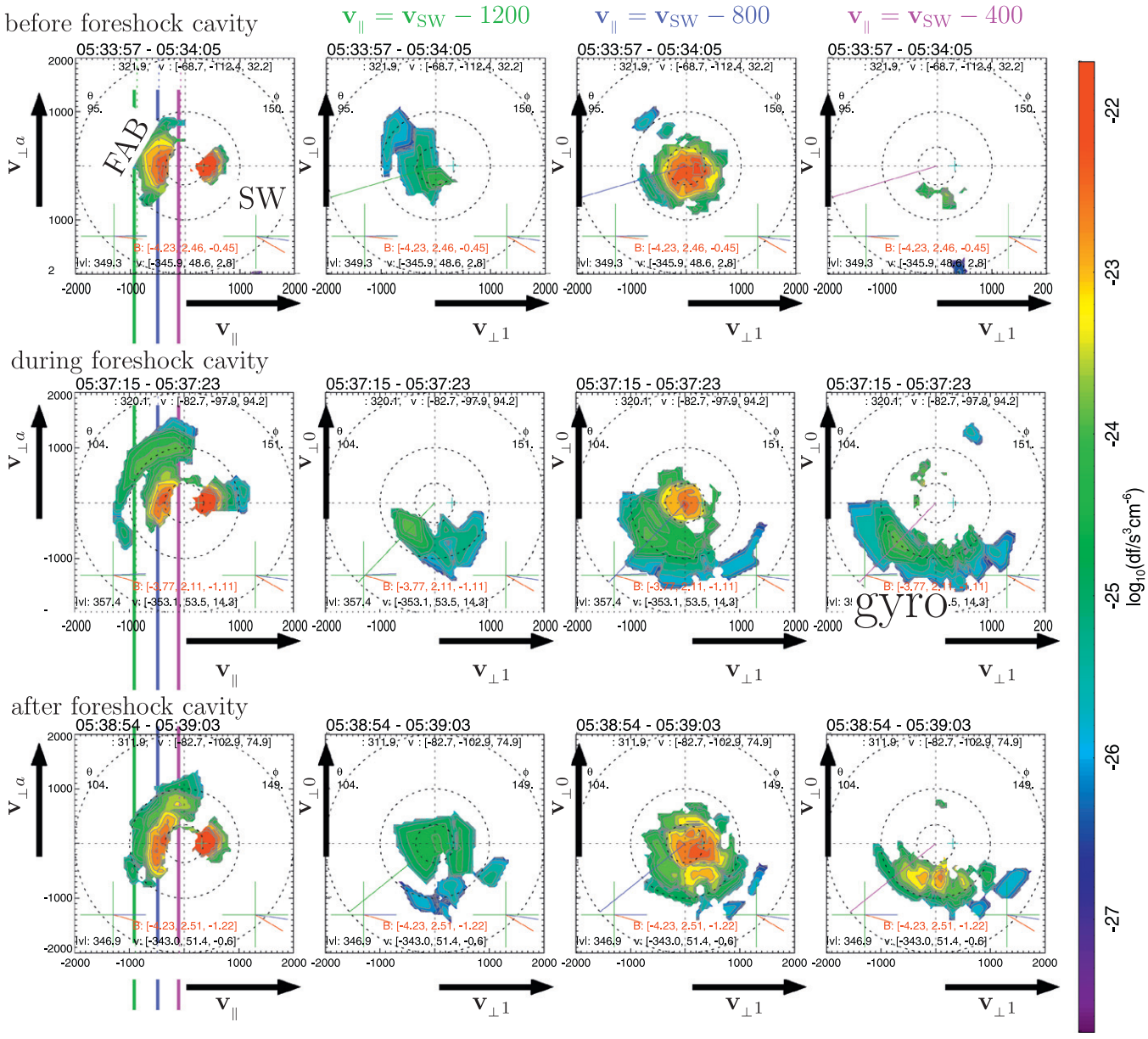

Fig. 5. Cuts through the ion distributions observed by the CIS(HIA) instrument on C1 between 2006-02-04 05:33 and 05:39. The distributions were calculated after subtracting off the perpendicular component of the bulk flow. Each row corresponds to a two spin gathering period centred at 05:34:01, 05:37:03 and 05:38:59; before, during and after the foreshock cavity, respectively. See text for explanation of the format. Other cuts are available from within the foreshock cavity, all show the new population (labelled 'gyro' here) in the same part of phase space; this suggests these ions may be phase trapped. The cuts presented are not contaminated by noise or adversely affected by asymmetric one-count thresholding.

on the far right. They appear in a 'u-shaped' arc (labelled 'gyro' in the rightmost column of the middle row), and extend out to velocities of several times that of the solar wind. Such signatures are characteristic of gyrophase-restricted, gyrating distributions. Within the foreshock cavity, all samples show this population. After the passage of the cavity this population persists for a few minutes; but does so intermittently. The gyrating component is most visible in periods of falling magnetic field magnitude. Under certain circumstances instrumental noise, factors such as asymmetric single count thresholding or time aliasing might mimic the signatures of gyrophase-restricted ions. However, the data presented here are not afflicted by such problems.

The signatures of the new ion component that appears inside the foreshock cavity bears some resemblance to the ring distribution of specularly reflected ions found gyrating in the foot of the bow shock (Möbius et al., 2001). As shown in Fig. 2, C4's encounter with the bow shock implies that C1 is near the bow shock.

The C1-shock distance perpendicular to the magnetic field is $\sim 0.9R_E$. This corresponds to one gyroradius (in the cavity interior field) of a proton with $\mathbf{v}_{\perp} = 2100\,\mathrm{km\,s^{-1}}$ or, equivalently, an energy of ~ 22 keV. Such perpendicular speeds are higher then those of the gyrating component in Fig. 5. For reference, an ion with 10 keV of kinetic energy (typical of the time series spectrum in the second panel of Fig. 3) would have a speed of $1384\,\mathrm{km\,s^{-1}}$. However, as the solar wind speed is only $350\,\mathrm{km\,s^{-1}}$, protons whose bulk flow energy was simply transformed into gyrational energy would not be expected gain more than ~ 700 eV; or, hence, to be found further than $\sim 10^3$ km from the bow shock (this is a function of θ_{Bn} and normal inflow speed: see Gosling and

Thomsen, 1985, for the full derivation). These factors suggest that the gyrating component inside the foreshock cavity is not simply part the ring distributions of reflected ions in the foot of the shock.

Other gyrating ion distributions are observed upstream of the shock. Field Aligned Beams, in the presence of the solar wind beam, are unstable to the ion-ion right hand resonant instability (e.g. Mazelle et al., 2003; Gary, 1991; Fazakerley et al., 1995). This instability generates waves which act, in turn, to disrupt the beams; producing gyrophase bunched ions. However, the lack of significant low frequency wave activity in the interval around the foreshock cavity, the persistence of the FAB component and the constancy of the observed gyrophases of the gyrating ions all argue against local production of the gyrating ions by beam disruption and phase trapping.

The distance between C1 and the shock along the cavity interior field is $\sim 1R_E$. In the 3 min after the cavity, during which the gyrating component is intermittent, the field aligned distance to the shock is nearly constant at $0.76 \pm 0.06R_E$. This suggests that the constancy of observed gyrophase is a spatial or geometrical effect.

Meziane et al. (2004) report the simultaneous observation of Field Aligned Beams and gyrating ions. The appearance of the gyrating ions was accompanied by the onset of large-amplitude Ultra Low Frequency fluctuations of the magnetic field. The two populations were found to be associated with adjacent field lines with the spacecraft encountering the (~ 1 gyroradius wide) boundary between escaping populations. We examine whether the ion signatures associated with this foreshock cavity are consistent with a similar situation. Does C1 sample the edge of a region of escaping reflected ions?

The velocity separation between the solar wind beam and upstream ion populations can be calculated for various ion production mechanisms. Ions specularly reflected from the shock will simply have their shock normal aligned velocity reversed and hence will be separated from the solar wind beam by $|\mathbf{v}_{SR}| = 2\mathbf{v}_{SW} \cdot \hat{\mathbf{n}}$. Ions that are effectively mirrored at the shock by a magnetic moment conserving process will have their velocities reversed in the de Hoffmann-Teller frame and emerge at a speed, relative to the solar wind, of $|\mathbf{v}_{\mu}| = 2\mathbf{v}_{SW} \cdot \hat{\mathbf{n}}/\cos\theta_{Bn}$. Table 1 shows $|\mathbf{v}_{SR}|$ and $|\mathbf{v}_{\mu}|$ computed for intervals corresponding to each row of Fig. 5. Before, during and after the foreshock cavity the velocity separation between FAB component and the solar wind beam is consistent with magnetic moment conserving mirroring from the shock. The gyrating ions observed inside the foreshock cavity and for a few minutes afterwards are too energetic to have been produced by specular reflection at the point where the magnetic field threading the spacecraft intersects the shock. However, the difference in the magnetic field signatures at the four Cluster spacecraft shows that there is structure in the field at scales of 10^4 km. Thus, energetic ions with finite pitch angles will sample regions of space having different field configurations. It is possible that the gyrating ions were 'launched' on a fieldline other than the one threading the spacecraft at the time of the ion observations as is the case for the event reported by Meziane et al. (2004). However, as the spacecraft are much closer to the shock than the shock's radius of curvature (Farris and Russell, 1994) nearby field lines are likely to connect to regions with similar $|\mathbf{v}_{SR}|$. This argues against the production of the gyrating population by specular reflection on nearby field lines.

Table 1
Velocity separation between the solar wind beam and reflected ions calculated for shock normal component reversing reflection and magnetic moment conserving mirroring.

Interval	$\lvert\mathbf{v}_{SR}\rvert$ (km s^{-1})	$\lvert\mathbf{v}_{\mu}\rvert$ (km s^{-1})
05:34:01	610 ± 95	960 ± 100
05:37:19	625 ± 100	1060 ± 110
05:38:58	605 ± 95	980 ± 100

The three rows correspond to the rows of Fig. 5.

In summary, the foreshock cavity observed by C1 is filled with a high energy gyrating ion population. This population is associated with a brief (at the spacecraft) connection to the quasi-parallel shock; transient quasi-parallel shock connection is one of the predictions of the 'classic' model of foreshock cavity formation (e.g. Schwartz et al., 2006). However, the Fermi process invoked to energise the cavity-central ions (e.g. Billingham et al., 2008; Sibeck et al., 2001) would not lead to gyrophase bunching. Another observation not accounted for in the anomalous connection model is the persistence of the gyrating ions, albeit at reduced energies, for several minutes after the passage of the magnetic cavity.

The next section is concerned with observations of a foreshock cavity that appears during the traversal of a large-scale foreshock boundary. The description of the 05:53 event analysed above as 'isolated' should be understood as a contrast to the foreshock boundary cavity. If it were possible to reconstruct the region of space containing the Cluster spacecraft, the event may not appear isolated as it does in time-series data. In any case, the presence of Field Aligned Beams around the 05:37 event show that it is not completely isolated from the contiguous foreshock.

3. Foreshock boundary cavity 09:33

3.1. Overview

Some five hours after the event reported above, the Cluster spacecraft observed another foreshock cavity. This second cavity clearly occurs on a boundary between two distinct plasma regions. Sibeck et al. (2008) suggest that foreshock cavities are encounters with compressional boundary of the global foreshock in motion; this event appears to be consistent with such an explanation.

Fig. 6 shows an hour of magnetic field, ion moments, probe potential and high energy ion flux data taken by the four Cluster spacecraft around the event at 09:33. Early in the interval all of the Cluster spacecraft observe magnetic fields and densities (or probe potentials) with large fluctuating components. The observed magnetic fields typically connect to the bow shock at quasi-parallel geometries; for example the average field direction measured by C1 between 09:26 and 09:31 has $\langle\theta_{Bn}\rangle = 37^{\circ} \pm 9^{\circ}$ based on scaling the Slavin and Holzer (1981) model to the nearest shock crossing at 08:00. Those spacecraft with working CIS(HIA) sensors observe perturbations to the bulk flow speed correlated with those in the magnetic field. Suprathermal ion fluxes ramp up during the early part of the interval, reaching a maximum around 09:33 when there is 35° duskward rotation of the magnetic field. Following this rotation magnetic field, ion moment and probe potential fluctuations are much reduced and the flux of suprathermal ions is negligible. The typical shock geometry during the interval 09:33–09:46 is $\theta_{Bn} \sim 70^{\circ}$.

The boundary between the disturbed and quiescent regions (crossed at 09:33:25 by C1) is marked by a clear ($\sim 80\%$) drop out in field magnitude and a $\sim 65\%$ drop in thermal ion density; this depleted region is filled with suprathermal ions. C2 observes the bounding field rotation 30 s later than C1 and measures a maximum in energetic ion flux coincident with a magnetic (50% depleted) and probe potential (70% depleted) cavity. These

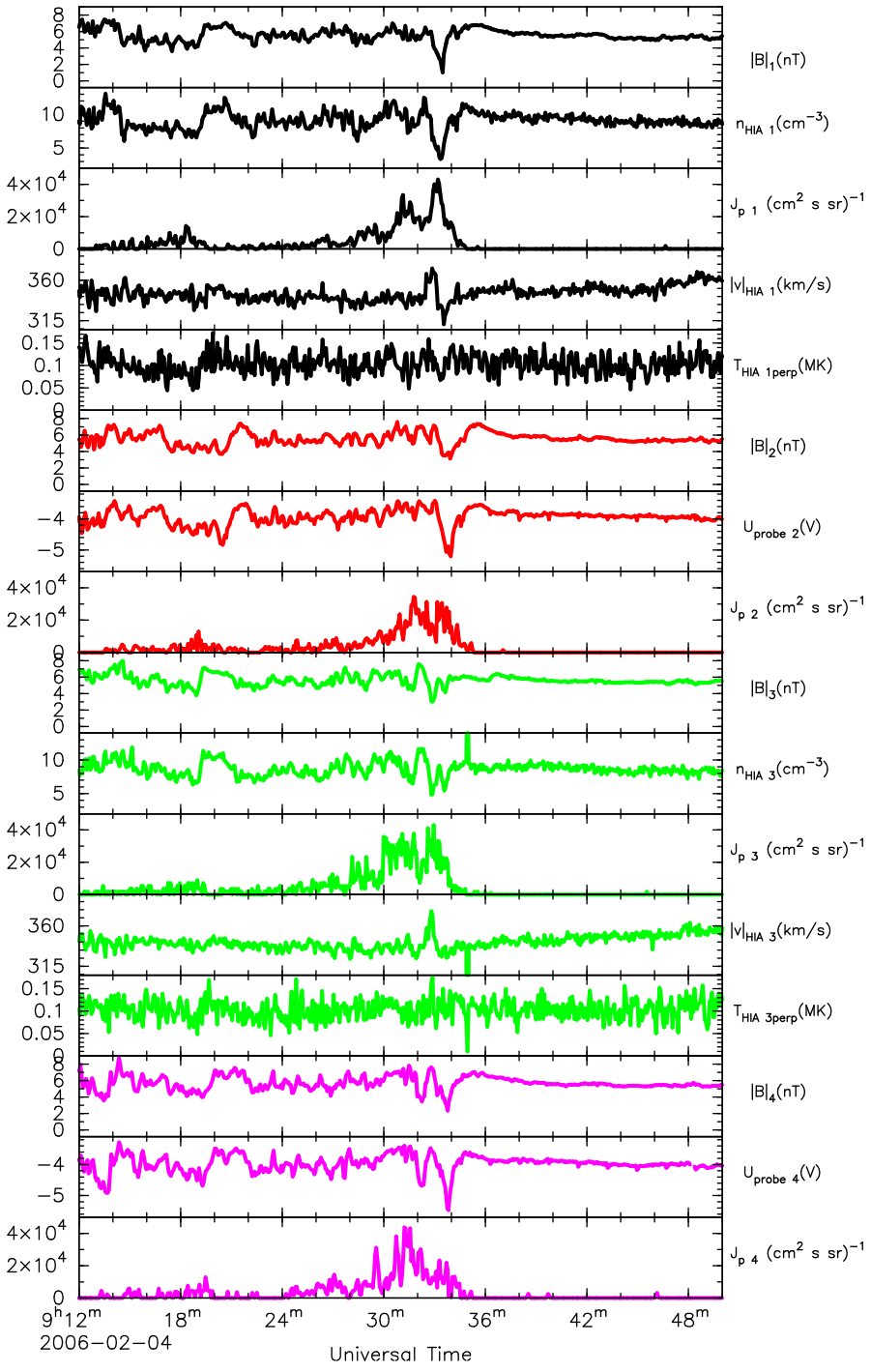

Fig. 6. Magnetic field thermal ion, probe potential and energetic ion data taken between 2006-02-04 09:12 and 09:50. For the C1 and C3 sub-stacks, the panels show (top to bottom) FGM magnetic field magnitude, CIS(HIA) ion density, RAPID suprathermal ion flux, CIS(HIA) bulk flow speed and CIS(HIA) ion temperature. For C2 and C4, EFW probe potential replaces density (for which it is a proxy) and ion flow speed and temperature are plots are omitted as the CIS(HIA) instruments on C2 and C4 are non-functioning. Cluster C1 and C2 observe clear depletions in magnetic field magnitude filled with suprathermal ions at 09:33. Signatures at C3 and C4 are more complicated and are discussed in the text. Conditions before the event clearly have larger amplitude fluctuations than those afterwards, suggesting the crossing of a boundary.

magnetic depletions measured at C1 and C2 are smoother and more pronounced than any of the fluctuations observed in the previous 20 min and easily distinguishable as unique events. At C3, the boundary is associated with correlated decreases in magnetic field magnitudes and densities to $\sim$55% of their values outside. There are two distinct depletion regions separated by an interior recovery. Similar twin magnetic and potential drop outs are measured at C4; however, the measured peak flux of suprathermal ions occurs before either of the two cavity-like structures.

The fourth-from-top and fifth-from-bottom panels of Fig. 6 show that there is some change in the bulk flow speed associated with the cavity. The variation is only at a level of 15%, which is below the threshold used by Billingham et al. (2008) to differentiate foreshock cavities from Hot Flow Anomalies. HFAs typically show decreased interior bulk flow speeds compared to

the surrounding solar wind (Schwartz et al., 2000), this event is associated with increased speeds. There are high fluxes of energetic (RAPID) ions associated with this event. The energy overlap between the CIS and RAPID instruments means that some change in the CIS moments is to be expected due to the presence of the high energy population.

This event, whilst fitting the usual selection criteria for a foreshock cavity, also resembles a foreshock density hole. These events, first reported by Parks et al. (2006) with follow up work by Wilber et al. (2008) and Lin et al. (2008), are often observed to be associated with moderate rotations in the magnetic field and small velocity deviations. Whilst most density holes are entirely embedded within quasi-parallel or oblique foreshock regions, a few have been identified coincident with transitions between quasi-parallel and quasi-perpendicular regimes. The question of whether this event is a density hole or a foreshock cavity hinges, not only on the possible overlap in the selection criteria for the two classes of event, but also on the nature of the underlying current sheet. Is the current sheet passive, simply affecting the transition between foreshock regions, or does it play an active role in the development of the suprathermal ion fluxes? We address this question in the next section.

3.2. Event details

Eight minutes of magnetic field observations around the foreshock cavity are presented in Fig. 7. The magnetic field magnitude traces differ greatly between spacecraft and within the

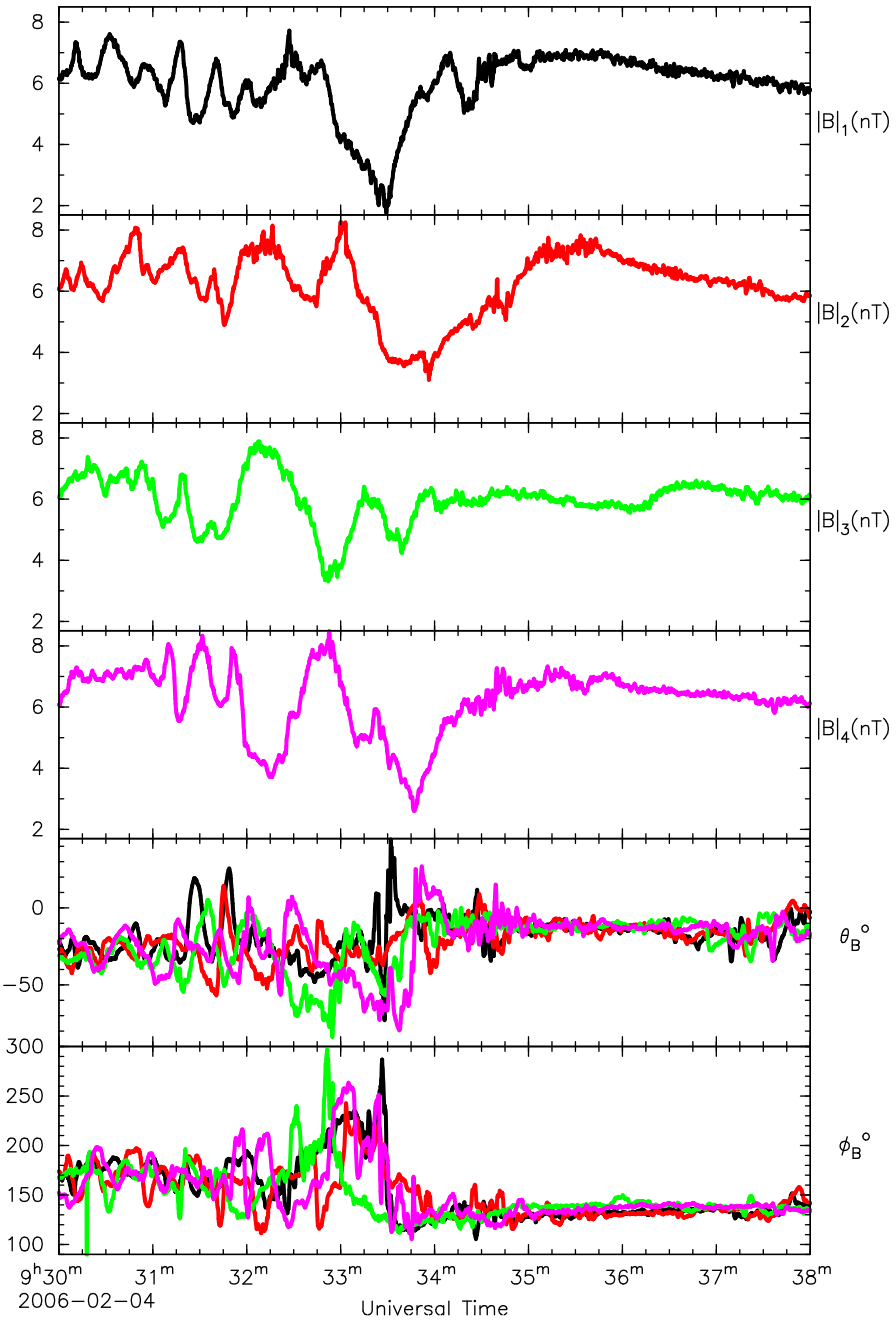

Fig. 7. Magnetic field data at 5 Hz resolution in the 10 min around the foreshock cavity. The first four panels show field magnitude from each spacecraft. The final panels show field latitudinal and azimuthal angles.

time series taken by a single spacecraft, the observations are highly structured on timescales of tens of seconds. The spacecraft are separated by $\sim 10^4$ km, corresponding to about one gyroradius for a 27 keV (RAPID energy range) proton in the cavity interior field. In general, the signatures of foreshock cavities seen by spacecraft separated by 10,000 km (Cluster 2006 dayside season) differ considerably. For this event, C3 and C4 observe several magnetic field dropouts of similar magnitude, whilst the signatures at C1 and C2 both have a single dominant cavity structure. Clearly, the upstream plasma has considerable structure on 10^4 km scales.

The relative timing of well-defined magnetic field features at the four Cluster spacecraft can be used to determine the orientation of the underlying magnetic structure and to diagnose its spatial extent without assuming it to be simply convecting in the solar wind (see e.g. Schwartz, 1998, and references therein).

The magnetic field profiles in Fig. 7 lack the obvious common characteristics required for timing analysis; these are also lacking from the clock angle and GSE component profiles which are not shown. The event also violates the assumption of time-stationarity required for timing analysis.

Other methods such as the assumption of an underlying tangential discontinuity (Burgess, 1995), or the use of the magnetic (Schwartz, 1998) or velocity (Abraham-Shrauner, 1972) coplanarity theorems give large variations in results; not only between differing methods, but when applying different up- and down-stream selection intervals within a given method. These problems mean that we cannot reliably determine the orientation or motion of underlying current sheet; and hence cannot conclude if it is active or passive. We rely on the diagnosing the width of this foreshock cavity under the assumption of pure solar wind convection and compare the event to the expectations based on a passive current sheet causing a foreshock crossing.

The magnetic depletion region in the Skadron et al. (1986) foreshock model has a width of $\sim 9R_E$. This is larger than the

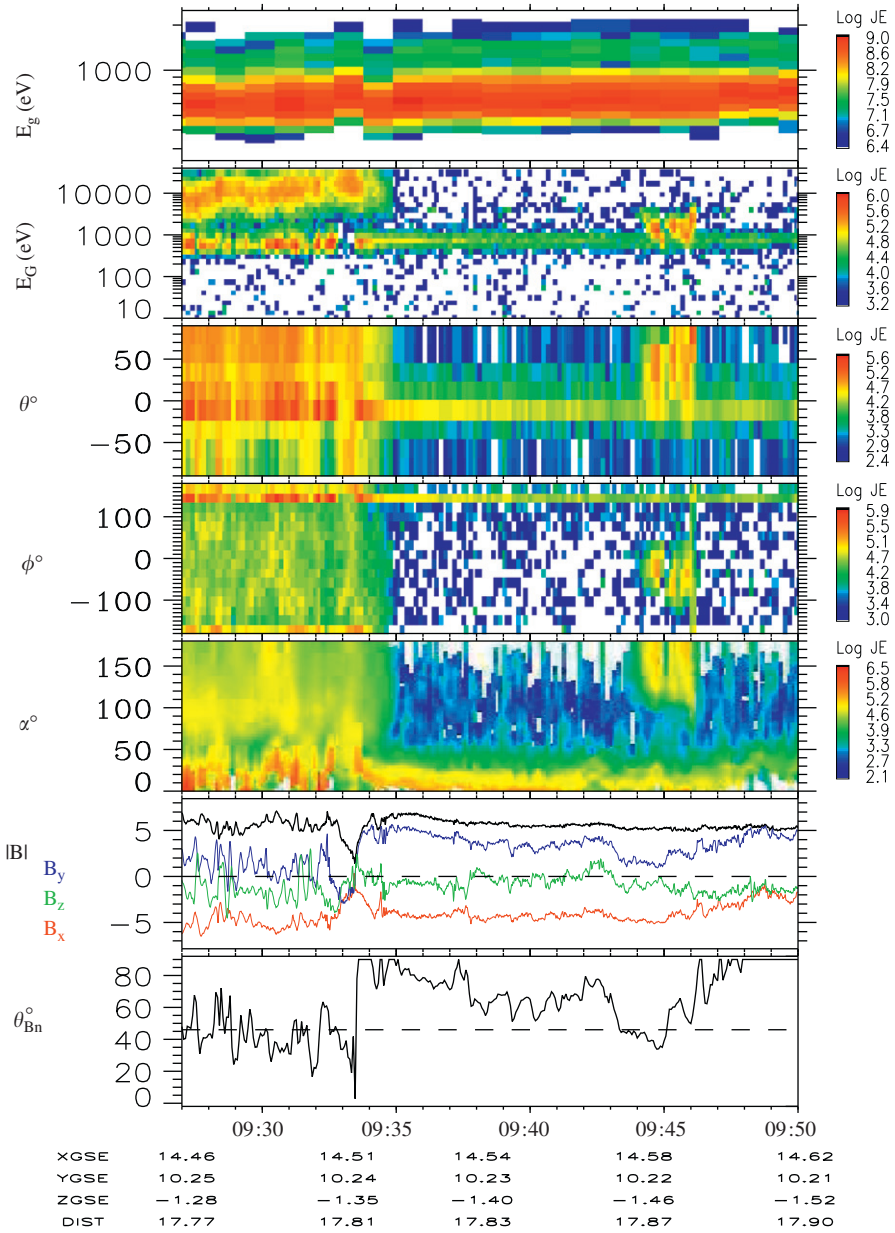

Fig. 8. Data from CIS(HIA) sensor taken between 2006-02-04 09:27 to 09:50 on C1. The format is similar to that of Fig. 3. However, there is an additional row showing the latitudinal flow angle, third from top.

$\sim 3R_E$ to the convected width of the 09:33 foreshock cavity. However, the width of the initial beam in the Skadron et al. (1986) simulations, along with the time allowed for the events to evolve, control the width of the depletion regions presented.

Fig. 8 clearly shows that this second foreshock cavity lies on the boundary between two different plasma populations. Before the event, Cluster observes large fluxes of ions incident from the quasi-parallel bow shock. The event bounds a moderate field rotation. The post-cavity shock geometry is $\theta_{Bn} \sim 70^{\circ}$. At such angles, it is typical to observe little ion flux incident from the shock (Meziane et al., 2005b).

These observations are consistent with a crossing from the foreshock into the solar wind. This crossing occurs as a result of a (35°) change in the direction IMF. Billingham et al. (2008) show that the majority of foreshock cavities, unlike the 09:33 event, are not associated with magnetic field discontinuities.

It appears that Sibeck et al. (2008) imagine foreshock cavities to be observed due to the back and forth motion of the boundary between the field-aligned ion beam or diffuse ion region and the solar wind, although they do not specify which part of the ion foreshock corresponds to the compressional boundary in their model. The signatures of this foreshock cavity presented in Fig. 8 show that the ions observed on the foreshock side of the boundary correspond to a wide range of pitch angles. However, the flux is not omnidirectional with less flux directed southward than northward. These features are more consistent with a traversal from the developed but not fully diffuse-ion foreshock to the electron foreshock or solar wind than an encounter with the FAB region.

4. Discussion and conclusions

Two foreshock cavity case studies were presented in this paper. One 'isolated' event was observed at two of the Cluster spacecraft whilst another spacecraft encountered the bow shock. This allowed, for the first time, an accurate diagnosis of the shock geometry and foreshock environment during the cavity encounter. This cavity was found to lie within a region of field-aligned ion beams. The event was associated with a region connected to the quasi-parallel bow shock which was embedded within a region of quasi-perpendicular connection. This local connection anomaly was associated with the appearance of an energetic, gyrating, ion population. This event mostly matches the classic model of foreshock cavity formation. However, more theoretical/simulational work should concentrate on the mechanism by which the cavity energetic ions are accelerated which remains an open question. A Fermi-type process modified to take place within a spatially restricted medium is one potential candidate.

The second 'boundary' foreshock cavity was observed when small magnetic field rotation caused the Cluster spacecraft to transition between two dissimilar plasma regimes. The spacecraft moved from the deep ion foreshock to region lacking backstreaming ions. This event had some similarities to a recent suggestion of Sibeck et al. (2008) that foreshock cavities are simply transient encounters with structures in the global foreshock. However, it occurs during a one-way transition rather than as a result of 'back-and-forth' motion. The lack of magnetic shear from before to after the foreshock cavities in the Billingham et al. (2008) survey suggests that boundary foreshock cavities are relatively rare compared to isolated cavity events. Future work should address the relationships between isolated and boundary foreshock cavities, the caviton events reported by Blanco-Cano et al. (2009) and the density holes of Parks et al. (2006) as there appears to be some ambiguity in the identification of foreshock transient events.

The boundary case study presented here occurs whilst Cluster exits the ion foreshock. It is not yet clear if similar signatures are observed during foreshock entry.

Most foreshock crossings result from changes in the IMF direction (Meziane and d'Uston, 1998). Studies of foreshock entry events and intervals where spacecraft motion, rather than IMF rotation, causes a foreshock crossing are needed to explain the appearance of boundary cavities. Comparisons of such intervals with foreshock transitions affected by current sheets should enable the distinctions to be drawn between passive foreshock transitions and active current sheets. The work of Skadron et al. (1986) suggests that boundary cavity signatures may be caused by pressure gradients caused by backstreaming ions. Attention should be paid to the changes in pressure that occur on the crossing of foreshock boundaries.

It is clear from the dissimilarities between the data taken at each of the four Cluster spacecraft during both events that the regions upstream of the bow shock may be highly structured on scales of 10,000 km. Studies of edge foreshock cavities using Cluster at smaller separations should enable the current sheet geometry to be diagnosed. With accurate event orientation and motion, studies of the interaction of the current sheet with the bow shock will enable the activity level of the current sheet to be determined.

Acknowledgements

The authors would like to thank the FGM (PIs: A. Balogh/E. Lucek), and CIS (PIs: H. Rème/I. Dandouras), EFW (PI: Mats André) and RAPID (PI: P. Daly) instrument teams, and the teams responsible for the Queen Mary Science Analysis System, and the Cluster Science Data System. This work was supported by UK STFC through the award of a studentship to LB and research grants to Imperial College London. Work at SSL is supported by NASA Grants NNG05GF99G and NASA-NNX07AP96G.

References

Abraham-Shrauner, B., 1972. Determination of magnetohydrodynamic shock normals. Journal of Geophysical Research 77, 736–739.

Balogh, A., Carr, C.M., a, M.H., AcuñDunlop, M.W., Beek, T.J., Brown, P., Fornaçon, K.-H., Georgescu, E., Glassmeier, K.-H., Harris, J., Musmann, G., Oddy, T., Schwingenschuh, K., 2001. The cluster magnetic field investigation: overview of in-flight performance and initial results. Annales Geophysicæ 19, 1207–1217.

Billingham, L., Schwartz, S.J., Sibeck, D.G., 2008. The statistics of foreshock cavities: results of a cluster survey. Annales Geophysicæ 26 (12), 3653–3667.

Blanco-Cano, X., Omidi, N., Russell, C.T., 2009. Global hybrid simulations: foreshock waves and cavitons under radial interplanetary magnetic field geometry. Journal of Geophysical Research (Space Physics) 114 (A13), 1216–+.

Bonifazi, C., Moreno, G. (Eds.), 1981a. Reflected and Diffuse Ions Backstreaming from the Earth's Bow Shock. Basic Properties, vol. 1, August.

Bonifazi, C., Moreno, G. (Eds.), 1981b. Reflected and Diffuse Ions Backstreaming from the Earth's Bow Shock. Origin, vol. 2, July.

Burgess, D., 1995. Collisionless shocks. In: Kivelson, M.G., Russell, C.T. (Eds.), Introduction to Space Physics. Cambridge University Press, Cambridge, pp. 129–164.

Eastwood, J.P., Lucek, E.A., Mazelle, C., Meziane, K., Narita, Y., Pickett, J., Treumann, R.A., 2005. The foreshock. Space Science Reviews 118, 41–94.

Farris, M.H., Petrinec, S.M., Russell, C.T., 1991. The thickness of the magnetosheath—constraints on the polytropic index. Geophysical Research Letters 18, 1821–1824.

Farris, M.H., Russell, C.T., 1994. Determining the standoff distance of the bow shock: mach number dependence and use of models. Journal of Geophysical Research 99, 17681–+.

Fazakerley, A.N., Coates, A.J., Dunlop, M.W., 1995. Observations of upstream ions, solar wind ions and electromagnetic waves in the Earth's foreshock. Advances in Space Research 15, 103–106.

Formisano, V., 1979. Orientation and shape of the Earth's bow shock in three dimensions. Planetary and Space Science 27, 1151–1161.

Fuselier, S.A., Thomsen, M.F., Gosling, J.T., Bame, S.J., Russell, C.T., 1986. Gyrating and intermediate ion distributions upstream from the Earth's bow shock. Journal of Geophysical Research 91, 91–99.

Gary, S.P., 1991. Electromagnetic ion/ion instabilities and their consequences in space plasmas—a review. Space Science Reviews 56, 373–415.
Gosling, J.T., Thomsen, M.F., 1985. Specularly reflected ions, shock foot thicknesses, and shock velocity determinations in space. Journal of Geophysical Research 90, 9893–9896.
Gosling, J.T., Thomsen, M.F., Bame, S.J., Russell, C.T., 1989. On the source of diffuse, suprathermal ions observed in the vicinity of the Earth's bow shock. Journal of Geophysical Research 94, 3555–3563.
Gustafsson, G., Bostrom, R., Holback, B., Holmgren, G., Lundgren, A., Stasiewicz, K., Ahlen, L., Mozer, F.S., Pankow, D., Harvey, P., Berg, P., Ulrich, R., Pedersen, A., Schmidt, R., Butler, A., Fransen, A.W.C., Klinge, D., Thomsen, M., Falthammar, C.-G., Lindqvist, P.-A., Christenson, S., Holtet, J., Lybekk, B., Sten, T.A., Tanskanen, P., Lappalainen, K., Wygant, J., 1997. The electric field and wave experiment for the cluster mission. Space Science Reviews 79, 137–156.
Kellogg, P.J., Horbury, T.S., 2005. Rapid density fluctuations in the solar wind. Annales Geophysicæ 23, 3765–3773.
Lin, N., Lee, E., Mozer, F., Parks, G.K., Wilber, M., Rème, H., 2008. Nonlinear low-frequency wave aspect of foreshock density holes. Annales Geophysicæ 26, 3707–3718.
Lucek, E.A., Horbury, T.S., Balogh, A., Dandouras, I., Rème, H., 2004. Cluster observations of hot flow anomalies. Journal of Geophysical Research (Space Physics) 109, 6207–+.
Mazelle, C., Meziane, K., Lequéau, D., Wilber, M., Eastwood, J.P., Rème, H., Sauvaud, J.A., Bosqued, J.M., Dandouras, I., McCarthy, M., Kistler, L.M., Klecker, B., Korth, A., Bavassano-Cattaneo, M.B., Pallocchia, G., Lundin, R., Balogh, A., 2003. Production of gyrating ions from nonlinear wave–particle interaction upstream from the Earth's bow shock: a case study from cluster-CIS. Planetary and Space Science 51, 785–795.
Mazelle, C., Meziane, K., Wilber, M., Le Quéau, D., 2005. Field-aligned and gyrating ion beams in a planetary foreshock. In: Li, G., Zank, G.P., Russell, C.T. (Eds.), The Physics of Collisionless Shocks: Fourth Annual IGPP International Astrophysics Conference, American Institute of Physics Conference Series, vol. 781, August, pp. 89–94.
Merka, J., Szabo, A., Narock, T.W., Richardson, J.D., King, J.H., 2005. Three decades of bow shock observations by IMP 8 and model predictions. Planetary and Space Science 53, 79–84.
Meziane, K., d'Uston, C., 1998. A statistical study of the upstream intermediate ion boundary in the Earth's foreshock. Annales Geophysicæ 16, 125–133.
Meziane, K., Mazelle, C., Lin, R.P., LeQuéau, D., Larson, D.E., Parks, G.K., Lepping, R.P., 2001. Three-dimensional observations of gyrating ion distributions far upstream from the Earth's bow shock and their association with low-frequency waves. Journal of Geophysical Research 106, 5731–5742.
Meziane, K., Wilber, M., Mazelle, C., LeQuéau, D., Kucharek, H., Lucek, E.A., Rème, H., Hamza, A.M., Sauvaud, J.A., Bosqued, J.M., Dandouras, I., Parks, G.K., McCarthy, M., Klecker, B., Korth, A., Bavassano-Cattaneo, M.B., Lundin, R.N., 2004. Simultaneous observations of field-aligned beams and gyrating ions in the terrestrial foreshock. Journal of Geophysical Research (Space Physics) 109, 5107–+.
Meziane, K., Wilber, M., Mazelle, C., Parks, G.K., Hamza, A.M., 2005a. A review of field-aligned beams observed upstream of the bow shock. In: Li, G., Zank, G.P., Russell, C.T. (Eds.), The Physics of Collisionless Shocks: Fourth Annual IGPP International Astrophysics Conference. American Institute of Physics Conference Series, vol. 781, August, pp. 116–122.
Meziane, K., Wilber, M., Mazelle, C., Parks, G.K., Hamza, A.M., 2005b. A review of field-aligned beams observed upstream of the bow shock. In: Li, G., Zank, G.P., Russell, C.T. (Eds.), The Physics of Collisionless Shocks: Fourth Annual IGPP International Astrophysics Conference. American Institute of Physics Conference Series, vol. 781, August, pp. 116–122.
Möbius, E., Kucharek, H., Mouikis, C., Georgescu, E., Kistler, L.M., Popecki, M.A., Scholer, M., Bosqued, J.M., Rème, H., Carlson, C.W., Klecker, B., Korth, A., Parks, G.K., Sauvaud, J.C., Balsiger, H., Bavassano-Cattaneo, M.-B., Dandouras, I., Dilellis, A.M., Eliasson, L., Formisano, V., Horbury, T., Lennartsson, W., Lundin, R., McCarthy, M., McFadden, J.P., Paschmann, G., 2001. Observations of the spatial and temporal structure of field-aligned beam and gyrating ring distributions at the quasi-perpendicular bow shock with cluster CIS. Annales Geophysicæ 19, 1411–1420.
Parks, G.K., Lee, E., Mozer, F., Wilber, M., Lucek, E., Dandouras, I., Réme, H., Mazelle, C., Cao, J.B., Meziane, K., Goldstein, M.L., Escoubet, P., 2006. Larmor radius size density holes discovered holes discovered in the solar wind upstream of Earth's bow shock. Physics of Plasmas 13, 050701–050705.
Paschmann, G., Sckopke, N., Papamastorakis, I., Asbridge, J.R., Bame, S.J., Gosling, J.T., 1981. Characteristics of reflected and diffuse ions upstream from the Earth's bow shock. Journal of Geophysical Research 86, 4355–4364.
Pedersen, A., Décréau, P., Escoubet, C.-P., Gustafsson, G., Laakso, H., Lindqvist, P.-A., Lybekk, B., Masson, A., Mozer, F., Vaivads, A., 2001. Four-point high time resolution information on electron densities by the electric field experiments (EFW) on cluster. Annales Geophysicæ 19, 1483–1489.
Pedersen, A., Lybekk, B., André, M., Eriksson, A., Masson, A., Mozer, F.S., Lindqvist, P.-A., Décréau, P.M.E., Dandouras, I., Sauvaud, J.-A., Fazakerley, A., Taylor, M., Paschmann, G., Svenes, K.R., Torkar, K., Whipple, E., 2008. Electron density estimations derived from spacecraft potential measurements on cluster in tenuous plasma regions. Journal of Geophysical Research (Space Physics) 113 (A12), 7–+.
Peredo, M., Slavin, J.A., Mazur, E., Curtis, S.A., 1995. Three-dimensional position and shape of the bow shock and their variation with Alfvenic, sonic and magnetosonic Mach numbers and interplanetary magnetic field orientation. Journal of Geophysical Research 100, 7907–7916.
Rème, H., Aoustin, C., Bosqued, J.M., Dandouras, I., Lavraud, B., Sauvaud, J.A., Barthe, A., Bouyssou, J., Camus, T., Coeur-Joly, O., Cros, A., Cuvilo, J., Ducay, F., Garbarowitz, Y., Medale, J.L., Penou, E., Perrier, H., Romefort, D., Rouzaud, J., Vallat, C., Alcaydé, D., Jacquey, C., Mazelle, C., d'Uston, C., Möbius, E., Kistler, L.M., Crocker, K., Granoff, M., Mouikis, C., Popecki, M., Vosbury, M., Klecker, B., Hovestadt, D., Kucharek, H., Kuenneth, E., Paschmann, G., Scholer, M., Sckopke, N., Seidenschwang, E., Carlson, C.W., Curtis, D.W., Ingraham, C., Lin, R.P., McFadden, J.P., Parks, G.K., Phan, T., Formisano, V., Amata, E., Bavassano-Cattaneo, M.B., Baldetti, P., Bruno, R., Chionchio, G., di Lellis, A., Marcucci, M.F., Pallocchia, G., Korth, A., Daly, P.W., Graeve, B., Rosenbauer, H., Vasyliunas, V., McCarthy, M., Wilber, M., Eliasson, L., Lundin, R., Olsen, S., Shelley, E.G., Fuselier, S., Ghielmetti, A.G., Lennartsson, W., Escoubet, C.P., Balsiger, H., Friedel, R., Cao, J.-B., Kovrazhkin, R.A., Papamastorakis, I., Pellat, R., Scudder, J., Sonnerup, B., 2001. First multispacecraft ion measurements in and near the Earth's magnetosphere with the identical Cluster ion spectrometry (CIS) experiment. Annales Geophysicæ 19, 1303–1354.
Scholer, M., 1995. Interaction of upstream diffuse ions with the solar wind. Advances in Space Research 15, 125–135.
Schwartz, S.J., 1998. Shock and discontinuity normals, mach numbers, and related parameters. In: Paschmann, G., Daly, P. (Eds.), Analysis Methods for Multi-Spacecraft Data ISSI Scientific Reports Series. ESA/ISSI Scientific Reports Series, pp. 249–270.
Schwartz, S.J., Paschmann, G., Sckopke, N., Bauer, T.M., Dunlop, M., Fazakerley, A.N., Thomsen, M.F., 2000. Conditions for the formation of hot flow anomalies at Earth's bow shock. Journal of Geophysical Research (Space Physics) 105, 12639–12650.
Schwartz, S.J., Sibeck, D., Wilber, M., Meziane, K., Horbury, T.S., 2006. Kinetic aspects of foreshock cavities. Geophysical Research Letters 33, 12103–+.
Sibeck, D.G., Decker, R.B., Mitchell, D.G., Lazarus, A.J., Lepping, R.P., Szabo, A., 2001. Solar wind preconditioning in the flank foreshock: IMP 8 observations. Journal of Geophysical Research (Space Physics) 106, 21675–21688.
Sibeck, D.G., Omidi, N., Dandouras, I., Lucek, E.A., 2008. On the edge of the foreshock: model-data comparisons. Annales Geophysicæ 26, 1539–1544.
Sibeck, D.G., Phan, T.-D., Lin, R., Lepping, R.P., Szabo, A., 2002. Wind observations of foreshock cavities: a case study. Journal of Geophysical Research (Space Physics) 107, 1–4.
Skadron, G., Holdaway, R.D., Scholer, M., 1986. Perturbation of the solar wind in a model terrestrial foreshock. Journal of Geophysical Research 91, 8798–8804.
Slavin, J.A., Holzer, R.E., 1981. Solar wind flow about the terrestrial planets. I—modeling bow shock position and shape. Journal of Geophysical Research 86, 11401–11418.
Thomas, V.A., Brecht, S.H., 1988. Evolution of diamagnetic cavities in the solar wind. Journal of Geophysical Research 93, 11341–11353.
Tjulin, A., Lucek, E.A., Dandouras, I., 2008. Wave activity inside hot flow anomaly cavities. Journal of Geophysical Research (Space Physics) 113 (A12), 8113–+.
Trattner, K.J., Möbius, E., Scholer, M., Klecker, B., Hilchenbach, M., Luehr, H., 1994. Statistical analysis of diffuse ion events upstream of the Earth's bow shock. Journal of Geophysical Research 99, 13389–+.
Wibberenz, G., Fischer, H.M., Zoellich, F., Keppler, E., 1985. Dynamics of intense upstream ion events. Journal of Geophysical Research 90, 283–301.
Wilber, M., Parks, G.K., Meziane, K., Lin, N., Lee, E., Mazelle, C., Harris, A., 2008. Foreshock density holes in the context of known upstream plasma structures. Annales Geophysicæ 26, 3741–3755.
Wilken, B., Daly, P.W., Mall, U., Aarsnes, K., Baker, D.N., Belian, R.D., Blake, J.B., Borg, H., Büchner, J., Carter, M., Fennell, J.F., Friedel, R., Fritz, T.A., Gliem, F., Grande, M., Kecskemety, K., Kettmann, G., Korth, A., Livi, S., McKenna-Lawlor, S., Mursula, K., Nikutowski, B., Perry, C.H., Pu, Z.Y., Roeder, J., Reeves, G.D., Sarris, E.T., Sandahl, I., Søraas, F., Woch, J., Zong, Q.-G., 2001. First results from the RAPID imaging energetic particle spectrometer on board Cluster. Annales Geophysicæ 19, 1355–1366.